Quantum order by disorder in a spin-one frustrated magnet on the kagome lattice

Sergei V. Isakov[1] and Yong Baek Kim[2]
[1]*Institute for Theoretical Physics, ETH Zürich, CH-8093 Zürich, Switzerland*
[2]*Department of Physics, University of Toronto, Toronto, Ontario, Canada M5S 1A7*
(Received 12 September 2008; revised manuscript received 21 January 2009; published 9 March 2009)

We study the *XXZ* spin-one quantum magnet with single-ion anisotropy on the kagome lattice as an example where quantum fluctuations on highly degenerate classical ground states lead to various exotic quantum ground states. Previous studies have predicted several quantum phases, but different analytical approaches do not necessarily lead to the same physical picture. In this work, we use quantum Monte Carlo computations to critically examine some of the predictions made in the string-net mean-field theory and the degenerate perturbation theory combined with duality analysis and effective-field theory. It is found that the resulting phase diagram differs from some of the previous predictions. Further implications of our results to different analytical approaches are discussed.

DOI: 10.1103/PhysRevB.79.094408 PACS number(s): 75.10.Jm, 71.27.+a, 75.40.Mg

I. INTRODUCTION

Macroscopic degeneracy of classical ground states in frustrated magnets is a fertile ground for emergence of unusual quantum ground states such as spiral magnetic order, quantum spin liquid, and valence bond solid (VBS) that occur via quantum fluctuations.[1] Any perturbation on the degenerate classical ground states, however, is inherently strong and there may also be more than one competing ground states that are extremely close in energy. The situation is very reminiscent of quantum Hall states that emerge from highly degenerate Landau levels. This is indeed one of the reasons why identification of true quantum ground state in frustrated magnets is such a difficult task.

Different kinds of nonperturbative analytical approaches have been proposed in literature to understand this quantum order (or disorder) by disorder phenomena. These approaches include various degenerate perturbation theories,[2] duality analysis combined with effective-field theories,[1,2] and string net condensation picture.[3] Since different approaches may not necessarily lead to the same conclusion, it is important to understand the limitations of various approaches. One useful way to obtain such information is doing unbiased numerics by appropriately choosing concrete examples where predictions from different approaches may vary.

Here we consider the following spin-one *XXZ* model with single-ion anisotropy on the kagome lattice as such an example.

$$H = -J_\perp \sum_{\langle ij \rangle} (S_i^x S_j^x + S_i^y S_j^y) + J_z \sum_{\langle ij \rangle} S_i^z S_j^z + D \sum_i (S_i^z)^2, \quad (1)$$

where $J_\perp$, J_z, $D>0$, the first two sums run over the nearest neighbors on the kagome lattice, and D is the strength of the single-ion anisotropy. This model is also equivalent to a boson model with nearest-neighbor repulsive interaction where boson occupation number can only assume 0, 1, and 2. Previously two different analytical approaches have been used to study the phase diagram of this model. Using degenerate perturbation theory and mapping to a dimer model combined with duality analysis, Xu and Moore[4,5] predicted that there exist three different phases: an *XY* ferromagnetic phase for $J_\perp \gg J_z$, D, a plaquette valence bond solid phase with resonating hexagons (VBS-H) for $J_\perp \ll D < J_z$, and a gapped "photon" (quantum paramagnetic) phase for $J_\perp \ll J_z < D$. The gapped photon phase is a descendant of an unstable two-dimensional quantum spin liquid phase with linearly dispersing neutral photon modes. It was also predicted that there would be a direct transition between VBS-H and a gapped photon phase. Using a quite different approach, Levin and Wen[6] proposed a mean-field theory where a class of variational wave functions based on the so-called "string-net" picture was used to map out the global phase diagram. While they also predict the existence of a plaquette phase as well as a gapped photon phase, their plaquette phase is characterized by frozen spin configurations and this frozen plaquette (FP) phase is different from VBS-H in lattice and spin symmetries.[6] In this string-net mean-field theory, the photon phase corresponds to the string-net condensed phase[6] and the unstable two-dimensional spin liquid phase mentioned above. This photon phase was found in a narrow region around $J_z \sim D$ if one ignored the nonperturbative instanton contribution. The photon excitation acquires a finite gap, however, due to the instanton effect in 2+1 dimensions.[6,7] The resulting state is an ordinary quantum paramagnetic state.

In this work, we map out the phase diagram of the model given by Eq. (1) using quantum Monte Carlo method. We use a plaquette generalization[8] of the stochastic series expansion algorithm.[9] We consider only the parameter region $J_\perp > 0$, $J_z > 0$, and $D > 0$. The schematic phase diagram is shown in Fig. 1. First, we find that a plaquette-ordered VBS phase indeed arises and it is the VBS-H phase not the FP. In addition to the phases discussed in the previous works, we also find an additional phase with resonating lattice units for small values of D/J_z and $J_\perp/J_z$. The ground state in this region is either a valence bond phase with resonating triangles (VBS-T) or a valence bond phase with resonating bow ties (VBS-B). It was argued in Ref. 5 that there should be a direct continuous transition from the VBS-H phase to the paramagnetic (gapped photon) phase. We do not observe such a transition for $J_\perp/J_z \gtrsim 0.08$. However, we cannot fully rule out the possibility of a direct VBS-H-paramagnet phase transition at even smaller values of $J_\perp/J_z$. We do not study

 ©2009 The American Physical Society

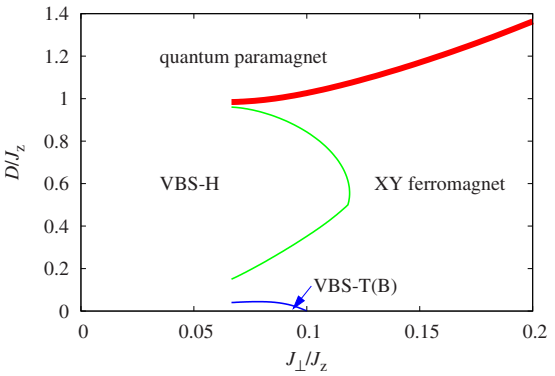

FIG. 1. (Color online) The phase diagram is based on Monte Carlo simulations. First-order phase transitions are denoted by thin lines (blue and green online) and a continuous phase transition is denoted by a thick line (red online).

the phase diagram for $J_\perp/J_z \lesssim 0.08$ as we experience problems with algorithm efficiency.

The rest of the paper is organized as follows. In Sec. II, we will discuss the details of the phase diagram and properties of all the phases discovered in the numerics. Here we also discuss the difference between our results and the predictions of previous works. We discuss the implications of our results to various analytical approaches in Sec. III.

II. CONSTRUCTION OF THE PHASE DIAGRAM

A. VBS-H phase

We begin with the analysis of the VBS-H phase that is found in a wide lobe as shown in Fig. 1. This phase has plaquette order. Two different plaquette phases were proposed previously for this region of parameters. In the plaquette phase (VBS-H) predicted by Xu and Moore,[4,5] spins resonate on a third of the total number of hexagons. These spins have $\langle S_i^z\rangle = b/2$ around resonating hexagons, where b is some number. The rest of the spins are fixed to $\langle S_i^z\rangle = -b$. In the FP phase predicted by Levin and Wen,[6] spins are frozen on a third of all the hexagons with alternating values of $\langle S_i^z\rangle = \pm a$ around those frozen hexagons; the rest of the spins has $\langle S_i^z\rangle = 0$.[6] Thus, these two phases break the Ising and lattice symmetries in different ways. Note that these two phases can also be distinguished by the distribution function of $\langle S_i^z\rangle$ (more discussions are given below).

In the resonating plaquette phase, the bond-bond correlation functions should have peaks in momentum space corresponding to the specific pattern in real space characterizing plaquette bond order. In Fig. 2, we show the bond-bond correlations function in real space that is given by

$$C_b(\mathbf{r}_\gamma - \mathbf{r}_\delta) = \left\langle \left[\frac{1}{\beta}\int B_{\gamma\tau} d\tau - B_0\right]\left[\frac{1}{\beta}\int B_{\delta\tau} d\tau - B_0\right]\right\rangle, \tag{2}$$

where $B_{\alpha(i,j),\tau} = J_\perp(S_i^x S_j^x + S_i^y S_j^y)$ is the off-diagonal bond operator (at imaginary time τ) of the bond α connecting spins i and j and B_0 denotes the background bond strength. In Fig. 2, one can clearly see the pattern that is compatible with the

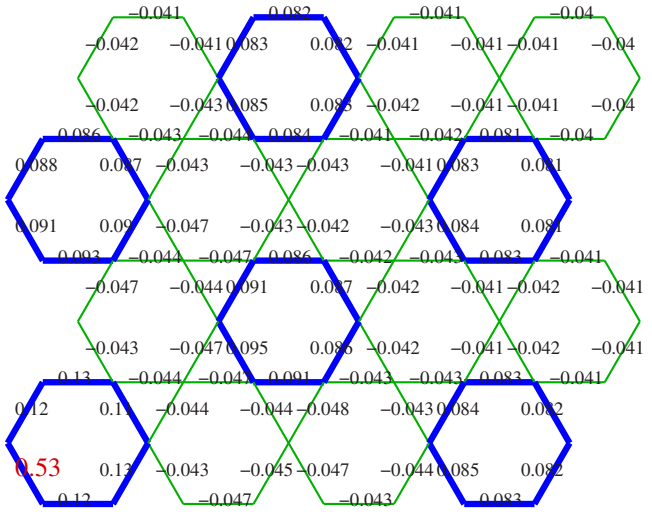

FIG. 2. (Color online) The correlation function $C_b(\mathbf{r}_1 - \mathbf{r}_\delta)$ between the bond indicated by a large text (red online) and the other bonds for $L=24$, $J_z/J_\perp = 10$, $D/J_z = 0.4$, and $T = J_\perp/48$. Resonating hexagons are denoted by thick lines.

VBS-H phase. To confirm that the bond order is long ranged, we show in Fig. 3 the finite-size scaling of the equal time bond-bond structure factor $S_b(\mathbf{q})$ at the ordering wave vector $\mathbf{q} = \mathbf{Q}_0 = (4\pi/3, 0)$,

$$S_b(\mathbf{q}) = N\langle B_{\mathbf{q}\tau}^\dagger B_{\mathbf{q}\tau}\rangle, \tag{3}$$

where $B_{\mathbf{q}\tau} = (1/N)\Sigma_\alpha B_{\alpha\tau}\exp(i\mathbf{q}\mathbf{r}_\alpha)$. Note that the expression of $B_{\mathbf{q}\tau}$ involves the sum over the bond index α, and N is the number of sites. The structure factor divided by the number of sites clearly goes to a finite value in the thermodynamic limit even though the extrapolated value is quite small.

On the other hand, the bond-bond correlation described in the previous paragraph might also be compatible with the FP phase. More robust diagnostic is the distribution function of local $\langle S_i^z\rangle$, which should have two peaks for the VBS-H phase and three peaks for the FP phase if the system is in one of the six degenerate symmetry-broken states.[10] For each Monte Carlo configuration, we compute the time-averaged $\bar{S}_i^z = (1/\beta)\int_0^\beta d\tau S_{i\tau}^z$, $S_{i\tau}^z$ is the z component of the spin operator at site i and imaginary time τ. In Fig. 4, the distribution

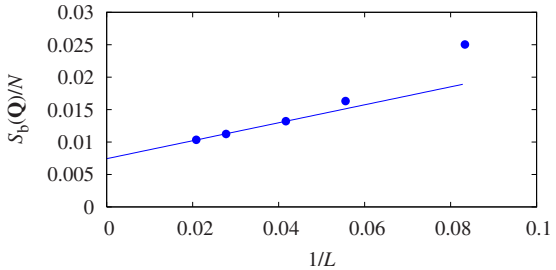

FIG. 3. (Color online) Finite-size scaling of the equal time bond-bond structure factor $S_b(\mathbf{Q}_0)$ for $J_z/J_\perp = 10$, $D/J_z = 0.4$, and $T = J_\perp/48$. In this and the other structure factor plots, error bars (if not visible) are smaller than the symbol sizes, and the line shows a linear extrapolation to the thermodynamic limit.

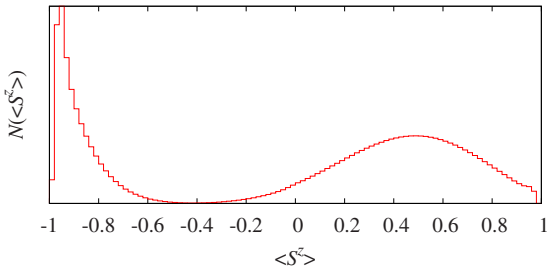

FIG. 4. (Color online) Probability distribution (arbitrary units) of $\bar{S}_i^z$ for $L=48$, $J_z/J_\perp=10$, $D/J_z=0.4$, and $T=J_\perp/48$. The distribution function is independent of the system size (not shown).

function of $\bar{S}_i^z$ is shown. The distribution function has two peaks; one sharp peak at $-b$ and the other broader peak at $b/2$. This is what we expect for the VBS-H phase. For the frozen plaquette phase, one expects three peaks at a, 0, and $-a$.

The VBS-H phase also has magnetic order. In Fig. 5, we show the finite-size scaling of the equal time spin-spin structure factor at $\mathbf{q}=\mathbf{Q}_0$,

$$S(\mathbf{q}) = N\langle S^\dagger_{\mathbf{q}\tau} S_{\mathbf{q}\tau}\rangle, \tag{4}$$

where $S_{\mathbf{q}\tau}=(1/N)\Sigma_i S^z_{i\tau}\exp(i\mathbf{q}\mathbf{r}_i)$.

Therefore, our Monte Carlo data are consistent with the resonating plaquette phase (VBS-H). It is worth noting that the VBS-H phase is quite similar to the VBS phase discovered in the hard-core boson model on the kagome lattice at fillings of 1/3 and 2/3 (for details, see Refs. 11 and 12).

B. VBS-T(B)

Another interesting result in this work is the discovery of another phase with resonating plaquettes at small values of $D/J_\perp$ and large values of $J_z/J_\perp$ as shown in Fig. 1. This phase was not predicted before. There are actually two different competing phases that are very close in energy. Triangles resonate in one of those phases (VBS-T phase) and bow ties resonate in the other one (VBS-B phase). We are not able to determine reliably which phase is the true ground state.

We find that there is a finite temperature transition from the high-temperature paramagnetic phase to the resonating phase for $J_z/J_\perp \geq 10$ and D close to zero. We have not attempted to obtain the precise location of this transition. The transition temperature $T_0 \approx J_\perp/10$ for $J_z/J_\perp=10.5$ and $D=0$. Typically, we find the VBS-T just below the transition and either the VBS-T or VBS-B phase at much lower temperatures depending on the configuration we start our Monte Carlo simulations with.

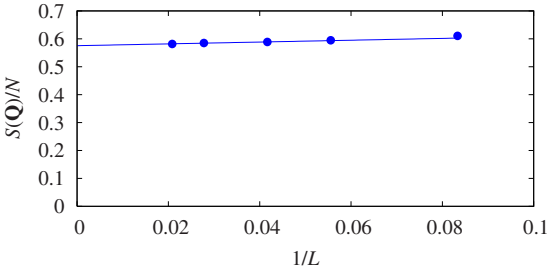

FIG. 5. (Color online) Finite-size scaling of the equal time spin-spin structure factor $S(\mathbf{Q}_0)$ for $J_z/J_\perp=10$, $D/J_z=0.4$, and $T=J_\perp/48$.

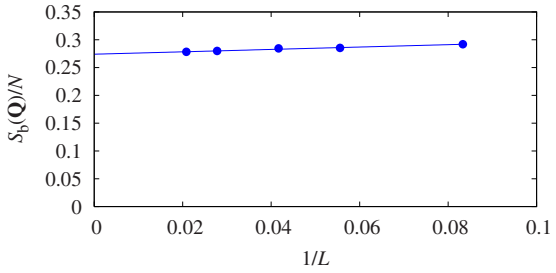

FIG. 6. (Color online) Finite-size scaling of the equal time bond-bond structure factor $S_b(\mathbf{Q}_3)$ for $J_z/J_\perp=10.5$, $D=0$, and $T=J_\perp/12$.

The bond-bond correlators have well-pronounced peaks at $\mathbf{Q}_1=(\pi,0)$, $\mathbf{Q}_2=(0,\pi)$, and $\mathbf{Q}_3=(\pi,\pi)$ in the VBS-T phase and at those and other symmetry-related points in the VBS-B phase. In Fig. 6, the finite-size scaling of the equal time bond-bond structure factor $S_b(\mathbf{Q}_3)$ defined in Eq. (3) is shown for the VBS-T phase. The structure factor divided by the number of sites scales to a finite value in the thermodynamic limit indicating long-range valence bond order. Note that the VBS order parameter is very large[13] in sharp contrast to the VBS-H bond order parameter and to some other models, in which the VBS order was confirmed in quantum Monte Carlo simulations.[11] To investigate the nature of the VBS-T(B) phase, we study the real-space correlation function defined in Eq. (2). As shown in Figs. 7 and 8, the VBS-T phase exhibits a network of resonating triangles and the VBS-B phase shows a network of resonating bow ties.

It is worth noting that the presence of the insulating phase at $D=0$ is in sharp contrast to the spin-1/2 XXZ model with

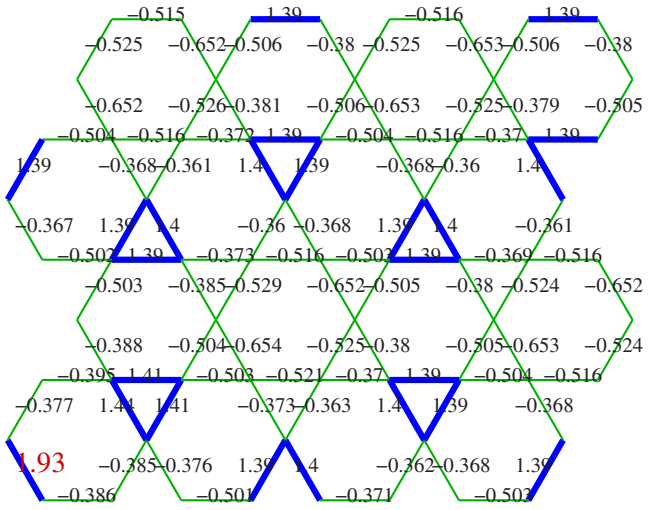

FIG. 7. (Color online) The correlation function $C_b(\mathbf{r}_1-\mathbf{r}_\delta)$ between the bond indicated by a large text (red online) and the other bonds for $L=12$, $J_z/J_\perp=10.5$, $D=0$, and $T=0.05J_\perp$. Resonating triangles (trimers) are denoted by thick lines.

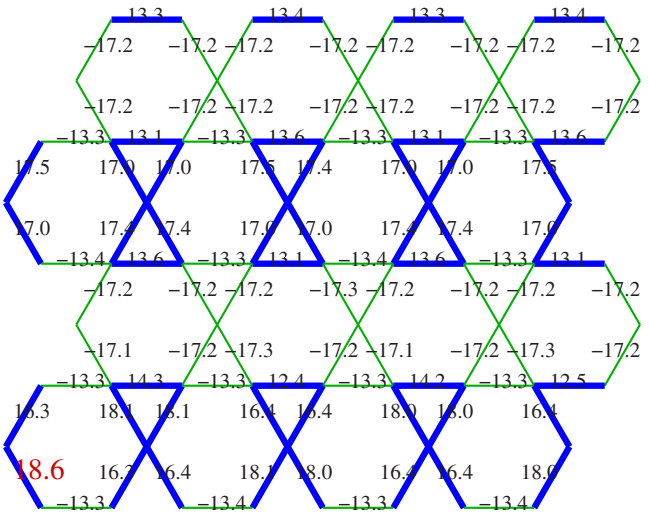

FIG. 8. (Color online) The correlation function $C_b(\mathbf{r}_1-\mathbf{r}_\delta)$ between the bond indicated by a large text (red online) and the other bonds for $L=12$, $J_z/J_\perp=10.5$, $D=0$, and $T=0.002J_\perp$. Resonating bow ties are denoted by thick lines.

ferromagnetic XY and antiferromagnetic Ising exchange interactions on the kagome lattice, where the uniform XY ferromagnet persists at any finite value of $J_\perp/J_z$.[11,12]

The appearance of the VBS-T or VBS-B state can be qualitatively explained as follows. Let us first consider the $D=0$ case. The classical model ($J_\perp=0$) has the ground-state constraint such that each triangle on the kagome lattice should have one of the spin arrangements $++-$, $+--$, or $+0-$ (and permutations), where the eigenvalues of the spin-1 S^z operator are denoted by $+$, $-$, and 0. There are many different ways to arrange classical spins on the lattice to fulfill the above constraint, leading to a highly degenerate classical ground-state manifold. The third group of states ($+0-$ and permutations) is quite special in the quantum case—a kinetic term (or an XY term) acting on such a state leaves the spins on a triangle (a flippable triangle) in the classical ground-state manifold; for example, $S_1^+S_2^-|0+-\rangle=|+0-\rangle$. In general, such a move may violate the classical ground-state constraint on the neighboring triangles. However, it does not violate the constraint in the special case when the three neighboring triangles of a flippable triangle have $+$ and $-$ spins as shown in Fig. 9. Thus the flippable triangles can resonate without leaving the classical ground-state manifold. This consideration naturally leads to the following wave function that has a kinetic-energy gain of $J_\perp$ (over the classical ground states) in first-order (degenerate) perturbation theory,

$$|\psi\rangle=|0+-\rangle+|0-+\rangle+|+0-\rangle+|-0+\rangle+|+-0\rangle+|0-+\rangle.$$

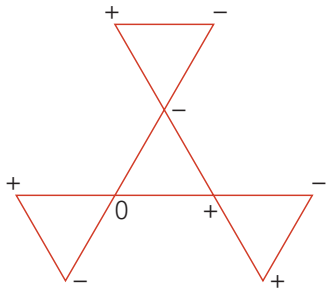

FIG. 9. (Color online) A sample configuration in which the central triangle can resonate without leaving the classical ground-state manifold.

On the other hand, two flippable triangles shown in Fig. 9 can resonate simultaneously giving rise to a resonating bow tie. It is expected that turning on an infinitesimal $J_\perp$ will favor the spin configurations where either the number of independently resonating triangles or the total number of resonating triangles is maximized. In the latter case, we expect that resonating bow ties are close packed as shown in Fig. 8. This arrangement of bow ties violates the classical ground-state constraint, and one needs to project out the components of the wave function that violate the constraint.[14] It is not possible to determine which state has lower energy based on the above analysis.

Therefore, quantum fluctuations lift the macroscopic degeneracy of the classical ground states and gives rise to a VBS phase via quantum order by disorder mechanism. The VBS phase should survive at small but finite values of D/J_z because of a finite excitation gap. The state with maximal number of independently flippable triangles is exactly the VBS-T state that is found in quantum Monte Carlo simulations, i.e., the configuration shown in Fig. 7. The spin configuration, where all the flippable triangles resonate, is the VBS-B phase and is shown in Fig. 8. The energies of those two states are very close.

As we have noted above, the bond order is very strong in the VBS-T(B) phase. This may be explained by the fact that the VBS-T phase can be chosen via resonating triangles in first-order perturbation theory, whereas, in most of other cases (including VBS-H), plaquette resonance is obtained in higher-order perturbation theory. As a result, the VBS-T(B) phase may be more robust than other cases.

C. Superfluid-paramagnet phase transition

In this subsection, we discuss the phase transition between the superfluid (or XY ferromagnet in spin language) and the featureless quantum paramagnet. Our numerics show that this transition is continuous and most likely belongs to the $3d$ XY universality class. We analyze the finite-size scaling of our data as follows. We measure the superfluid density by measuring the winding number fluctuations.[15] In the vicinity of a continuous transition, the superfluid density scales as

$$\rho_s=L^{-z}F_{\rho_s}[L^{1/\nu}(K_c-K),\beta/L^z], \tag{5}$$

where F_{ρ_s} is the scaling function, L is the linear system size, z is the dynamical critical exponent, ν is the correlation length exponent, $K_c-K=(D/J_z)_c-D/J_z$ is the distance to the critical point, and β is the inverse temperature. To cross the phase boundary, we change D and keep J_z fixed. The data scale very well with the dynamical critical exponent $z=1$. In Fig. 10, the superfluid density ρ_s times the system size L is shown as a function of the coupling constant. As follows from the above scaling form, the curves for different system sizes should cross at the transition point if the ratio β/L^z is

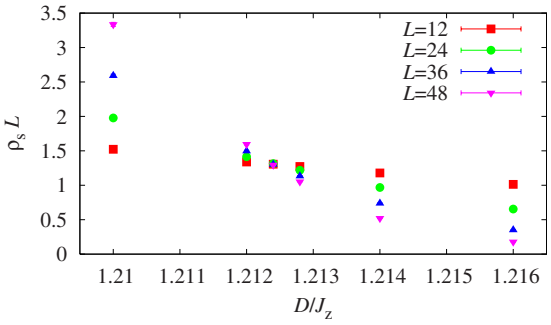

FIG. 10. (Color online) Finite-size scaling of the superfluid density ρ_s at $J_z/J_\perp=6$ for $\beta/L=1/J_\perp$.

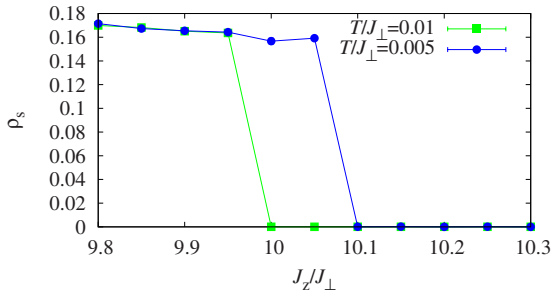

FIG. 12. (Color online) The superfluid density ρ_s as a function of $J_z/J_\perp$ for $L=12$, $D=0$, and different temperatures. Lines are guides to the eyes.

fixed. Such a distinct crossing point is seen at $(D/J_z)_c=1.2124$. It also follows from Eq. (5) that the curves for different system sizes should collapse onto a universal curve for appropriate values of ν and $(D/J_z)_c$ when $\rho_s L$ is plotted as a function of $[(D/J_z)_c-D/J_z]L^{1/\nu}$. In Fig. 11, we show such a data collapse for $\nu=0.67(2)$ and $(D/J_z)_c=1.2124(2)$. The error bars are estimated from the stability of the data collapse with respect to varying the fitting parameters. Thus one may conclude that the superfluid-paramagnet quantum phase transition is continuous. One may also infer that the transition is in the $3d$ XY universality class from $\nu=0.67(2)$. However, we have not measured the other critical exponents that could be used to unambiguously confirm this prediction.

D. Superfluid-VBS phase transitions

The quantum phase transitions out of the superfluid phase to VBS phases are strongly first order. As an example, let us consider the transition from the superfluid phase to the VBS-T phase. In Fig. 12, we show the superfluid density ρ_s as a function of $J_z/J_\perp$ at different temperatures. The superfluid density jumps at large values of $J_z/J_\perp$ indicating a transition to an insulating phase (VBS-T phase). We confirm that the transition is strongly first order by observing hysteresis effects upon increasing or decreasing $J_z/J_\perp$ across the transition (not shown) and by a double-peaked structure in the distribution of the XY energy (kinetic energy of bosons), $J_\perp\langle S_i^x S_j^x+S_i^y S_j^y\rangle$, close to the transition (not shown).

The transition from the superfluid phase to the VBS-H phase is also first order. In the top part of the VBS-H lobe (see Fig. 1), the first-order nature becomes somewhat weaker as the value of $J_\perp/J_z$ is decreased. We do not observe a direct transition from the VBS-H phase to the quantum paramagnetic phase, which was predicted in Ref. 5, in the parameter region we can access, i.e., for $J_\perp/J_z \gtrsim 0.08$. There is a narrow region of the superfluid phase between those two phases, as shown in Fig. 1. However, we cannot rule out the possibility that there might be a direct transition at much smaller values of $J_\perp/J_z$.

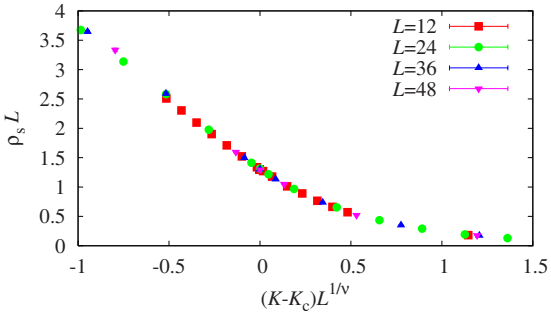

FIG. 11. (Color online) Data collapse of the superfluid density ρ_s at $J_z/J_\perp=6$ for $\beta/L=1/J_\perp$.

III. DISCUSSION

We now discuss possible origins of the discrepancy between our quantum Monte Carlo results and those of previous analytic approaches with various approximation schemes.[4–6] In particular, it is found that the VBS-H phase, not the FP, is the stable ground state for moderate strength of D/J_z and small $J_\perp/J_z$. This suggests that the string-net mean-field theory analysis in a previous work[6] may not be sufficient for the identification of the true ground state.

The string-net picture starts from an alternative representation of the spins on the kagome lattice, where the spins are considered to be in the middle of the links connecting the sites of the honeycomb lattice (that can be obtained by connecting the centers of triangles on the kagome lattice).[6] This honeycomb lattice is a bipartite lattice and consists of A and B sublattices. The occupation of a given link $I=\langle ij\rangle$ by a string is defined as follows: the link contains an oriented string pointing from $i\in A$ to $j\in B$ if $S_I^z=+1$ and from j to i if $S_I^z=-1$. The link is empty if $S_I^z=0$. Then the spin configurations on the original kagome lattice and those of oriented closed strings are in exact correspondence.[6]

The string-net mean-field theory uses the following ansatz for the variational ground-state wave function.[6] Here,

$$\Psi_z(X)=\prod_{ij} z_{ij}^{n_{ij}}, \tag{6}$$

where X represents an oriented string configuration and $\{z_{ij}\}$ represents a large number of variational parameters, and n_{ij} represents the occupation number of the oriented link ij. The mean-field analysis begins with a (translationally invariant) string liquid state (or a string condensed state) where z_{ij} can be set to a constant α. Considering the spectrum of collective modes in this state and the identification of the wave vector where the collective modes become soft, one can in principle

study the instability to a translational-symmetry-broken state. More explicitly, this can be achieved by writing $z_{ij} = \alpha e^{E_{ij}+iA_{ij}}$ and studying the fluctuations of E_{ij} and A_{ij}. It was found that the soft mode is described by $E=\Phi E_{+\mathbf{Q}}+\Phi^* E_{-\mathbf{Q}}$ and $A=0$, where $E_{\mathbf{Q}}$ is the Fourier mode at $\mathbf{Q}=(4\pi/3,0)$ and equivalent wave vectors.[6] Here Φ is a complex number.

The energy (or the Ginzburg-Landau theory) of the system as a function of Φ can be obtained as[5,6]

$$H(\Phi) = A|\Phi|^2 + B|\Phi|^4 + C[\Phi^6 + (\Phi^*)^6] + \ldots, \qquad (7)$$

where A, B, and C are real constants and Φ can be regarded as an order parameter. The choice of the ground state is sensitive to the phase of Φ and hence the sign of C basically determines the true ground state. It was found that if C is positive (negative), then the FP (VBS-H) is favored.[6] This sign, however, is very difficult to determine in analytic approaches. In Ref. 6, an unrestricted variational wave-function calculation was also done on a small system size 3×3, leading to the conclusion that the ground state may be the FP phase.[6] We think, however, that this system size is perhaps too small for definitive conclusion. Indeed our quantum Monte Carlo results are clearly consistent with the VBS-H phase, and hence the negative sign of C in the Ginzburg-Landau theory.

ACKNOWLEDGMENTS

This work was supported by the NSERC, CRC, CIFAR, KRF (Grant No. 2005-070-C00044), and the Swiss National Science Foundation (S.V.I.). We thank Cenke Xu, Joel Moore, Michael Levin, Xiao-Gang Wen, and Matthias Troyer for helpful discussions.

[1] For a review of possible quantum phases, see S. Sachdev, Ann. Henri Poincare **4**, 637 (2003).
[2] L. Balents, M. P. A. Fisher, and S. M. Girvin, Phys. Rev. B **65**, 224412 (2002); M. Hermele, M. P. A. Fisher, and L. Balents, *ibid.* **69**, 064404 (2004).
[3] X.-G. Wen, Phys. Rev. B **68**, 115413 (2003).
[4] C. Xu and J. E. Moore, Phys. Rev. B **72**, 064455 (2005).
[5] C. Xu and J. E. Moore, Phys. Rev. B **76**, 104427 (2007).
[6] M. Levin and X.-G. Wen, Phys. Rev. B **75**, 075116 (2007).
[7] A. M. Polyakov, Nucl. Phys. B **120**, 429 (1977).
[8] K. Louis and C. Gros, Phys. Rev. B **70**, 100410(R) (2004).
[9] A. W. Sandvik, Phys. Rev. B **59**, R14157 (1999); O. F. Syljuåsen and A. W. Sandvik, Phys. Rev. E **66**, 046701 (2002).
[10] On the time scale of our quantum Monte Carlo simulations, the system stays in one of the six degenerate symmetry-broken states. However, the finite-size system should fluctuate between different degenerate states on much longer Monte Carlo time scales.
[11] S. V. Isakov, S. Wessel, R. G. Melko, K. Sengupta, and Y. B. Kim, Phys. Rev. Lett. **97**, 147202 (2006).
[12] K. Damle and T. Senthil, Phys. Rev. Lett. **97**, 067202 (2006).
[13] K. S. D. Beach and A. W. Sandvik, Phys. Rev. Lett. **99**, 047202 (2007).
[14] R. Moessner and S. L. Sondhi, Phys. Rev. B **63**, 224401 (2001).
[15] E. L. Pollock and D. M. Ceperley, Phys. Rev. B **36**, 8343 (1987).